The Potential of Low-cost Millimeter-Wave Sensors for Mobile Radar Applications

Bernhard Großwindhager
Department of Electrical and Information Engineering
Graz University of Technology, Austria
grosswindhager@tugraz.at

***Abstract*—The millimeter-wave (mmWave) spectrum has emerged as a promising option to fulfill the need for high-speed links in future 5G cellular networks due to the high bandwidth available in these frequency bands. Besides future communication systems, also radar systems will highly benefit from the high bandwidth, as the latter results in a high time resolution enabling precise range estimations. Furthermore, the increased carrier frequency in mmWave systems enables packed and highly directive antenna arrays. This paves the way for several new applications such as motion monitoring, gesture recognition, and indoor mapping. Recently, the first single-chip mmWave radar solutions appeared on the market, which will facilitate the design of low-cost and mobile radar systems. This report investigates the properties and capabilities of low-cost mmWave sensors and acts as a reference for researchers and system designers working with mmWave radar sensors. The IWR1642 chip from Texas Instruments' mmWave sensor family is chosen to discuss low-level parameters of mmWave platforms and their applicability as tuning knobs to maximize the performance and reliability of mobile radar systems. Nevertheless, the remarks are platform-agnostic. Depending on the application requirements and the environmental conditions, optimal parameter sets are suggested and backed up with measurements in an indoor environment.**

***Index Terms*—mmWave, IWR1642, FMCW, radar.**

I. Introduction

After the observations of Heinrich Hertz in 1886 that radio waves are reflected by metallic objects, the German inventor Christian Hülsmeyer presented in the early 20th century the world's-first radar system to detect ships using continuous waves (CW) [1]. Due to its importance for military operation, researchers all over the world intensified their efforts to improve radar systems before World War II. The focus was primarily on pulsed radar system. Later on, frequency-modulated continuous-wave (FMCW) radar technology became increasingly popular. In contrast to CW radars, FMCW radars are modulating the transmitted signal with a known sequence (e.g., a sawtooth pattern), which increases the reliability, provides velocity as well as distance measurements, and allows to differentiate between multiple reflecting objects. The recent shift towards the millimeter-wave (mmWave) spectrum (> 30 GHz) for FMCW radars enables highly precise range estimates to targeted objects due to the high bandwidth available in these frequency bands. Furthermore, the reduced wavelength enables the application of small-sized MIMO antenna arrays allowing to precisely scan the environment and to resolve the angular domain with fine granularity. These inherent properties of mmWave radar systems and the recent availability of small and low-cost single-chip radar solutions operating in the mmWave band enabled plenty of new applications, such as human motion monitoring [2], vital signs monitoring [3], unmanned aerial vehicle and robot radar [4], gesture recognition [5], radar for autonomous cars and driving assistance systems [6] as well as power-line detection over the air and in walls [7].

Furthermore, mmWave radars are a promising technology for mobile indoor mapping. Current techniques to map indoor environments are typically based on mechanically-steered laser or optical sensors [8], which are bulky and restrict the system's portability and mobility. Moreover, these systems are much more susceptible to environmental influences such as light, heat, smoke and dust than mmWave-based systems. This makes the latter highly applicable for first responders as they often require accurate and up-to-date maps, i.e., taking into account structural changes due to the emergency, to rescue injured and locked-in people. Accurate indoor maps are also beneficial for indoor localization systems, e.g., in [9] accurate map information is required to exploit multipath reflections from walls instead of multiple physical anchors, however, the authors ignored the derivation of the map information. Due to the limited availability of hardware and the high costs for measurement equipment in the mmWave frequency bands, academic research in terms of environmental and indoor mapping using millimeter-wave radar was mainly focused on simulations [10] or specialized equipment [11], [12].

Recent low-cost mmWave radar sensors such as the IWR1642 chip from TI's mmWave sensor family, instead, enable the development of portable and handheld devices for indoor mapping and numerous other applications. This report highlights the potential of these low-cost mmWave sensors and supports researchers and system designers on designing reliable mobile radar applications. Sect. II discusses the basic principle of FMCW radars and the techniques to estimate the range, velocity, and angle of arrival. Next, the IWR1642 radar sensor and the evaluation board as well as the provided framework to acquire radar data is explained in Sect. III. The principle of FMCW radars provides numerous system parameters, which are introduced in Sect. IV. A guideline to select these parameters and how to apply them as tuning knobs to optimize the performance and reliability of radar applications depending on their requirements and the environmental conditions is discussed in Sect. V. The report concludes with a description of the provided measurement data in Sect. VI as well as of the required calibration steps in Sect. VII.

II. Working Principle of FMCW Radars

The basic principle of a radar is to transmit electromagnetic waves and to measure the signal reflected by objects to determine their range, velocity, and angle. FMCW radars transmit frequency-modulated signals, where the frequency typically increases linearly over time, resulting in a so-called linear chirp. The latter is defined by its start frequency (f_S), bandwidth (B), and duration (T_c). The echo received after a time delay τ is mixed with the transmitted chirp resulting in an intermediate frequency (IF) signal proportional to τ. Based on this signal, the FMCW radar is able to estimate the distance from the detected object (Sect. II-A), its velocity (Sect. II-B), as well as the angle of arrival (Sect. II-C).

A. Range estimation

Single object. In the case of a single reflecting object, the received (RX) chirp is a time-delayed version of the transmitted (TX) chirp (see Fig. 1). The time delay τ encodes the distance between the radar and the reflecting object as

$$\tau = \frac{2d}{c} \tag{1}$$

where d is the distance to the detected object and c is the speed of light in air. Assuming that the radar and the object are at fixed positions, the resulting intermediate frequency signal $s_{IF}(t)$ is a sine wave with a constant frequency f_0 and an initial phase Φ_0.

$$s_{IF}(t) = sin(2\pi f_0 t + \Phi_0) \tag{2}$$

with

$$f_0 = S\tau = \frac{B}{T_c} \cdot \frac{2d}{c}\ , \tag{3}$$

$$\Phi_0 = 2\pi f_S \tau = \frac{4\pi d}{\lambda_S} \tag{4}$$

and λ_S being the wavelength of the start frequency f_S. Thus, the frequency of the IF signal f_0 is defined by the slope of the chirp S and the time delay τ, whereas the initial phase Φ_0 is defined as the phase difference between the TX and RX signal at the start of the IF signal. Please note that the IF signal is just valid when the TX and RX signal are overlapping, marked with the vertical dotted lines in Fig. 1.

Mulitple objects. In the case of different reflecting objects, multiple time-delayed chirps will be received. Due to the different distances, the time delay will be different, resulting in multiple IF signals, each of which with a constant frequency, as shown in Fig. 1 (right). Fast Fourier transform (FFT) is used to separate the multiple tones: this FFT reveals the range of the reflecting objects and is also referred to as *range-FFT*.

Range resolution. Especially in indoor environments, the range resolution, i.e., the capability to separate objects lying close to each other, is a critical property for radar systems. Rearranging Eq. (3), one can estimate the distance between the radar and an object d as

$$d = \frac{T_c c}{2B} f_0 \tag{5}$$

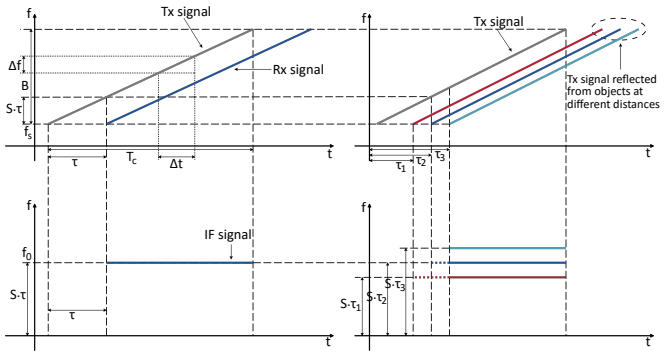

Fig. 1: Generation of intermediate frequency (IF) signal(s) for one (left) and multiple objects (right). The grey line denotes the transmitted chirp and the colored lines the chirps reflected from the objects (top). Mixing the received and the transmitted signal results in the IF signal(s) (bottom).

which results in a range resolution δd as a function of the frequency resolution δf_0 of the IF signals

$$\delta d = \frac{T_c c}{2B} \delta f_0. \tag{6}$$

The frequency resolution δf_0 is related to the length of the IF signal and hence the chirp duration T_c with $\delta f_0 \approx 1/T_c$ [13]. Inserting this relation in Eq. (6) results in

$$\delta d \approx \frac{T_c c}{2B} \frac{1}{T_c} = \frac{c}{2B}. \tag{7}$$

Hence, the range resolution δd is determined by the chirp bandwidth B. Due to the high bandwidth available in mmWave radar sensors, a range resolution of a few centimeters is possible. For example, the TI IWR1642 sensor features a maximum bandwidth of $B = 4\,\text{GHz}$, resulting in a range resolution of $\delta d \approx 3.75\,\text{cm}$. Please note that the range resolution also depends on other properties such as the chirp linearity [13], but these are out of the scope of this report.

B. Velocity estimation

To support mobile applications, it is a stringent requirement of mmWave radars to estimate the velocity of surrounding objects accurately. In the following, it is differentiated between estimating the velocity of a single object and estimating the velocity of multiple objects at the same range.

Single object. To estimate the radial velocity of an object, i.e., the velocity in the radial direction relative to the radar, two consecutive chirps separated by T_c are analyzed. Typically, the objects are traveling just a small distance Δd_v between two consecutive chirps, which results in the same range estimate due to the limited range resolution. In the frequency domain, this implies that the IF signals lie in the same bin of the Fourier transform. Hence, the spectrum will contain peaks at the same position but with different phase [14], as illustrated in Fig. 2. The phase difference Φ_v can be derived from Eq. (4) by applying the distance difference $\Delta d_v = v_r T_c$:

$$\Delta\Phi_v = \frac{4\pi\Delta d_v}{\lambda_S} = \frac{4\pi v_r T_c}{\lambda_S}. \tag{8}$$

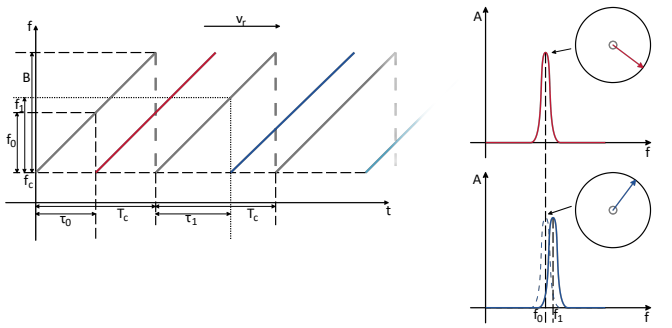

Fig. 2: Schematic of the velocity estimation in FMCW radars with a single object. A sequence of chirps is sent (left), resulting in the same spectral components (assuming that $f_0 \approx f_1$), but a different phase due to a slight movement (right).

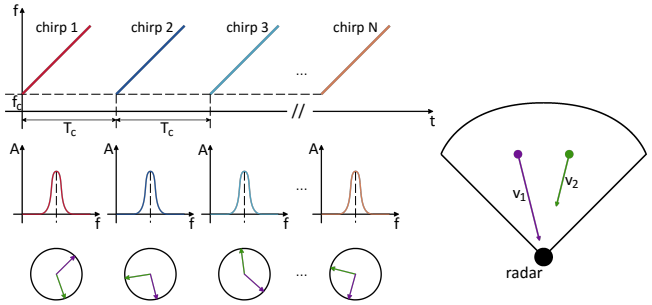

Fig. 3: A set of N chirps is transmitted (top left) to estimate N *range-FFTs* containing frequency/range and phase information (bottom left). The results are symbolically shown for two objects at the same distance to the radar, but with different speed v_1 and v_2, respectively (right). Because of the same distance, the peaks are at the same frequency, however, the phase information differs due to the different speed.

Hence, the radial velocity follows as

$$v_r = \frac{\lambda_S \Delta\Phi_v}{4\pi T_c}. \tag{9}$$

To unambiguously determine the radial velocity v_r, the phase shift $\Delta\Phi_v$ has to be $|\Delta\Phi_v| < \pi$, thus, the maximum relative velocity $v_{r,max}$ is

$$v_{r,max} = \frac{\lambda_S}{4T_c}. \tag{10}$$

Hence, to increase $v_{r,max}$, it is required to shorten the transmission time between the frequency chirps T_c.

Given that a change in phase over time relates to a frequency, one can link the previous observations to the Doppler effect via the Doppler angular frequency ω_d and the Doppler frequency shift f_d [15]:

$$\omega_d = 2\pi f_d = \frac{\Delta\Phi_v}{\Delta t} = \frac{4\pi}{\lambda_S} \cdot \frac{\Delta d_v}{\Delta t} = \frac{4\pi v_r}{\lambda_S}. \tag{11}$$

Substituting $\Delta t = T_c$, Eq. (8) follows from Eq. (11) and the Doppler shift f_d can be defined as

$$f_d = \frac{2v_r}{\lambda_S} = \frac{2v_r f_S}{c}. \tag{12}$$

Multiple objects at the same distance. The previously described two-chirp method, i.e., the transmission of two consecutive chirps to estimate the velocity of an object, does not work in situations where multiple objects with different speeds are at the same distance from the radar. The range-FFT, indeed, would just contain a single peak resulting from the combined reflected signal from all equidistant objects [14]. To resolve these multiple objects, N consecutive chirps (chirp frame) need to be sent. This concept is illustrated in Fig. 3 (top), which shows the frequency over time for a chirp frame containing of multiple chirps.

After the transmission of the chirp frame, a set of N *range-FFTs* is available, containing distance and phase information. Fig. 3 shows the resulting range-FFTs with two objects at a similar distance from the radar, but with different speeds v_1 and v_2, respectively. Because of the same distance, the peaks are at the same frequency for all chirps, but the phase information differs. The latter depends on the phase of both reflected signals, indicated with the two phasors (green and purple color in Fig. 3) for each range-FFT. By applying a second FFT (*Doppler-FFT*), it is possible to extract information about the Doppler angular frequency (ω_1, ω_2) for each object. Thus, the multiple chirps allow to separate the objects and consequently extract their individual velocity by employing Eq. (11).

$$v_1 = \frac{\lambda_S \omega_1}{4\pi} \text{ and } v_2 = \frac{\lambda_S \omega_2}{4\pi}. \tag{13}$$

After applying both the *range-FFT* and the *Doppler-FFT* a two-dimensional Range-Doppler-Matrix is constructed, which contains range and velocity information of detected objects. This matrix is used to derive the range/Doppler heatmap and the detection matrix $\mathbf{A}$, as discussed in Sect. VI.

C. Angle of arrival estimation

The antenna array available at mmWave radar sensors enables the estimation of the angle of arrival (AoA) of a reflected signal. The general principle is to measure the distance differences between the object and the individual antennas of the antenna array. These differences are measurable as phase changes in the FFT. The latter is referred to as *angle-FFT* or *azimuth-FFT*. Fig. 4 illustrates the principle of angle of arrival estimation with one object, one transmit antenna (tx), and two receive antennas (rx_1, rx_2). The phase difference at the receive antennas $\Delta\Phi$ follows from the distance difference Δd between the antennas and the object as

$$\Delta\Phi = \frac{2\pi\Delta d}{\lambda}. \tag{14}$$

Assuming a planar wavefront, one can relate the distance of the receive antennas l with the angle of arrival Θ via the difference Δd as $\Delta d = l \cdot sin(\Theta)$ (see Fig. 5). Substituting Δd in Eq. (14) results in the following equation for the angle of arrival Θ

$$\Theta = \arcsin\left(\frac{\lambda\Delta\Phi}{2\pi l}\right). \tag{15}$$

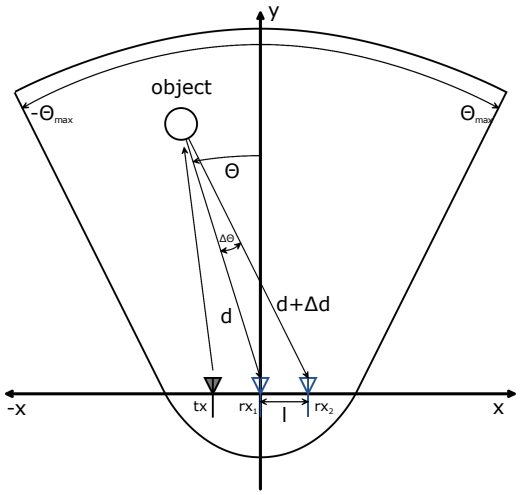

Fig. 4: Principle of angle of arrival Θ estimation with one object, one transmit antenna (tx), and two receive antennas (rx_1, rx_2). The different positions of the receive antennas cause a phase difference, which has to be detected.

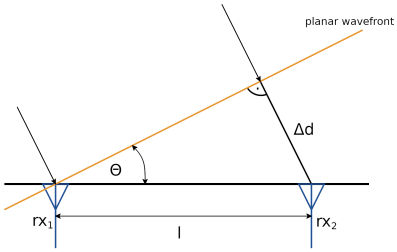

Fig. 5: Under the assumption that the distance of the receive antennas l is small compared to the distance to the object, simple trigonometry allows to derive the angle of arrival Θ.

Since the phase difference $\Delta\Phi$ can only be estimated unambiguously in the range $[-\pi, \pi]$ the maximum field of view Θ_{max} is defined by

$$\Theta_{max} = \pm \arcsin\left(\frac{\lambda}{2l}\right). \tag{16}$$

Hence, the maximum field of view of $\Theta_{max} = \pm 90°$ is achieved when the antennas are separated by $l = \lambda/2$ [16].

Please note that the relation between the measured phase difference $\Delta\Phi$ and the estimated angle of arrival Θ is not linear (see Eq. (15)), hence, the accuracy of the estimation is not constant for all angles. Indeed, the estimation is most accurate for small angles (close to 0°) and worst for angles close to 90°.

III. Hardware and Software Framework

Recently, several semiconductor companies have started their own product lines of 77 GHz single-chip radar sensors. Among others, these are Texas Instruments' mmWave sensor family [17] and Infineon's RASIC front-end ICs for automotive radars [18]. Texas Instruments differs between automotive mmWave sensors [19] and industrial mmWave sensors [20]. Since the focus of this report is mainly on indoor applications, the industrial mmWave sensor and specifically the IWR1642

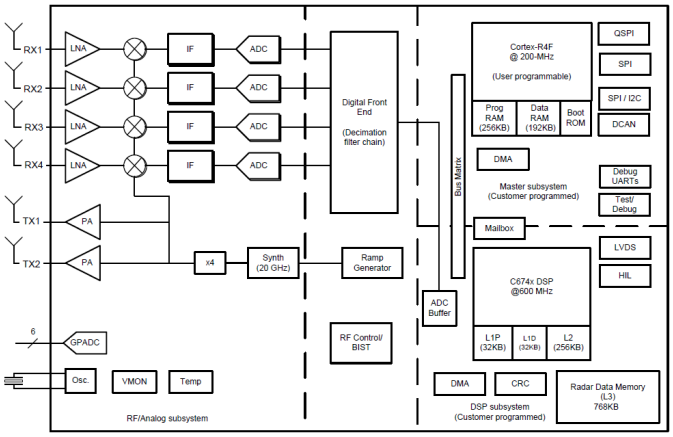

Fig. 6: Block diagram of TI IWR1642 (adapted from [21]). Additionally to the master subsystem containing a Cortex-R4F processor, the IWR1642 provides a C674x DSP to perform advanced signal processing tasks.

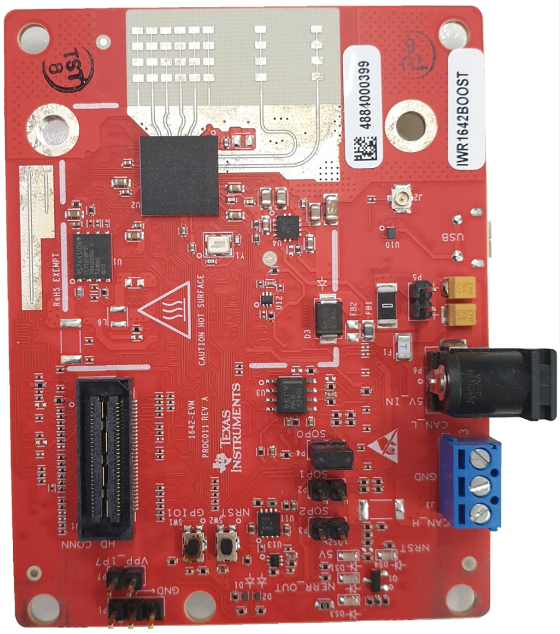

Fig. 7: Front view of the IWR1642BOOST evaluation board. At the top of the board is the PCB antenna array connected to the four receiver and two transmitter ports, respectively. The board is powered via a 5-V power connector.

FMCW mmWave sensor [21] is employed. However, the bulk of this report contains information that is applicable for all mmWave FMCW radar solutions.

This section discusses the hardware characteristics of the IWR1642 chip and its evaluation board. Furthermore, it gives a short overview of the used software framework.

Hardware. The IWR1642 radar chip covers the 76-81 GHz band and allows to select either a wide band with a chirp bandwidth of 4 GHz (77-81 GHz) or a narrow band with a bandwidth of 1 GHz (76-77 GHz). The radar front-end contains two transmitters (for transmit beamforming) and four receivers that can operate simultaneously as a MIMO radar.

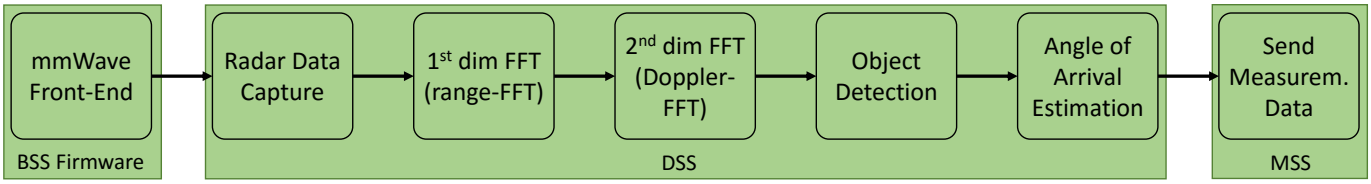

Fig. 8: Data path processing chain of the Texas Instrument IWR1642. The BSS firmware controls the mmWave front-end. It is followed by the DSP subsystem (DSS), which captures the radar data and estimates the range, velocity, and angle of arrival of detected objects. The firmware running on the Cortex-R4F (MSS) provides the measurement data for further processing.

As shown in the block diagram in Fig. 6, the IWR1642 also integrates, besides an ARM Cortex-R4F processor to configure and control the mmWave front-end, a C674x digital signal processor (DSP) allowing to run advanced signal processing algorithms (e.g., FFT, detection algorithms) [21][1].

The IWR1642 can be easily used with its IWR1642BOOST evaluation board from Texas Instruments [22] (see Fig. 7). It constains the required hardware and software packages to develop applications for the IWR1642 sensor. Furthermore, it contains a small PCB antenna array as shown in Fig. 7. The antenna is aligned to support measurements in the two-dimensional plane. Please note that the evaluation board of the IWR1443 also supports object detection in the 3-D plane [23]. The IWR1642BOOST evaluation board moreover features a LVDS interface to provide raw ADC data via the DCA1000EVM real-time data capture card [24]. The latter enables to stream the ADC data over Ethernet.

Software Framework. Texas Instruments provides a comprehensive software framework to work with the IWR1642 mmWave sensor. Within this report, the mmWave Software Development Kit (SDK) v01.02.00.05 is used (due to compatibility issues of the employed Rev.A evaluation board with newer versions of the SDK). The SDK is downloadable from the TI website[2]. Besides the SDK, one also requires the standalone flash tool *Uniflash*[3] and TI's *Code Composer Studio (CCS)*[4]. For the remainder of this report, the `xwr16xx_mmw_demo.bin` image in the SDK under `...\packages\ti\demo\xwr16xx\mmw` is used. It consists of the firmware running on the Cortex-R4F (master subsystem, MSS), the DSP code (DSP subsystem, DSS), as well as a separate firmware to control the RF/analog subsystem (BSS). This is highlighted in the data path processing chain of the IWR1642 software framework shown in Fig. 8. The processing chain consists of the steps discussed in Section II: (i) range-FFT and Doppler-FFT to estimate range and velocity, (ii) object detection, (iii) and angle of arrival estimation. These algorithms are running on the DSP subystem of the IWR1642 radar chip. After the detection of the targets using the DSP, the Cortex-R4F is responsible for providing the measurement data (see Sect. VI) via the UART interface.

[1]The DSP is not integrated in the IWR1443, i.e., an alternative chip from the TI industrial mmWave family operating in the same frequency band as the IWR1642, that is why the IWR1642 sensor was selected for this report.

[2]http://www.ti.com/tool/MMWAVE-SDK

[3]http://www.ti.com/tool/UNIFLASH

[4]http://www.ti.com/tool/CCSTUDIO

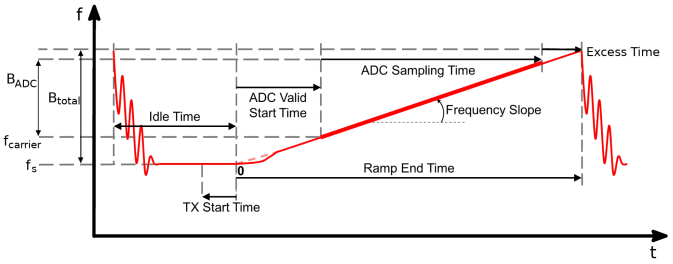

Fig. 9: Schematic of a chirp in FMCW radars and its configuration parameters (adapted from [26]). Each of these parameters influences the performance of the radar system.

IV. Configurable Parameters of FMCW Radar

FMCW mmWave radar sensors provide researchers and developers with numerous configuration parameters, which are applicable as tuning knobs to optimize the performance and reliability of mobile radar applications. For this purpose, one has to take the physical characteristics of the environment into account. This might enable runtime adaptation of mmWave configuration parameters similar to other wireless technologies providing a bandwidth in the GHz-range, such as Ultra-wideband transceivers [25]. The very good time resolution due to the high bandwidth enables to detect, among others, non-line-of-sight situations and destructive interference.

This section discusses the main configuration parameters affecting the transmit signal of FMCW radar sensors. The parameters can be categorized in settings affecting the chirp profile (Sect. IV-A) as well as the frame profile (Sect. IV-B). Sect. IV-C discusses the influence of these parameters on performance metrics such as range resolution, velocity resolution, maximum detectable range, and maximum relative velocity.

A. Chirp Profile

A chirp profile defines the basic properties of a frequency chirp. Up to four different profiles can be stored on the IWR1642 chip. The main properties to be set for the chirp are listed below and marked in Fig. 9. Note that this is just a selection of parameters: for the full list, please refer to the mmWave SDK User Guide [26]. In the SDK the `profileCfg` and `chirpCfg` commands are used to configure the chirp profile.

- **Start frequency** f_S
  Defines the starting frequency of the chirp ramp in GHz. Typically this is set to 77 GHz in order to exploit the wide band from 77-81 GHz for highest time resolution.

- **Idle time** T_{idle}
  Time between the end and start of a chirp in μs.
- **ADC valid start time** $T_{ADC,valid}$
  Time from the start of the frequency chirp ramp until valid samples are available at the ADC in μs.
- **Ramp end time** $T_{ramp,end}$
  Duration of the chirp ramp in μs. Consequently, the chirp cycle time $T_{c,c}$ is defined as $T_{c,c} = T_{idle} + T_{ramp,end}$ and the chirp repetition period $T_{c,r}$ as $T_{c,r} = N_{TX} \cdot T_{c,c}$, where N_{TX} is the number of TX antennas.
- **Frequency slope** S
  Defines the slope of the chirp in MHz/µs. The maximum value is 100 MHz/µs for the IWR1642 chip.
- **TX start time** $T_{TX,start}$
  Time of transmitter start relative to the ramp start in μs.
- **ADC sampling frequency** $f_{ADC,s}$
  ADC sampling frequency of the IF signal in ksps.
- **Number of ADC samples** $N_{ADC,s}$
  Total number of collected ADC samples during the ADC sampling time $T_{ADC,s}$. The ADC sampling time is defined by $T_{ADC,s} = N_{ADC,s}/f_{ADC,s}$. Furthermore, the number of range-FFT bins R depends on the number of ADC samples $N_{ADC,s}$ and follows as $R = 2^{\lceil log_2 N_{ADC,s} \rceil}$.

The transmitter is turned on $T_{TX,start}$ before the ramp starts. At this time, the frequency stays constant at the start frequency f_S and raises linearly after $T_{TX,start}$. The slope of the ramp is defined by the frequency slope S. After a guard time $T_{ADC,valid}$, the ADC sampling process is started and lasts for $T_{ADC,s}$. The latter is defined by the ADC sampling frequency $f_{ADC,s}$ and the number of ADC samples $N_{ADC,s}$. After another guard period, the chirp reaches its maximum frequency depending on the start frequency f_S and the total available bandwidth. Afterwards, the frequency returns to f_S and the transmitter is turned off and remains idle for T_{idle}.

B. Frame Profile

As discussed in Sect. II, velocity estimation with FMCW radars requires not just one, but a sequence of the previously defined frequency chirps. This sequence is called a frame. Additionally to the parameters of the individual chirps defined in Sect. IV-A, one can set the following parameters of the frame to adapt to the environmental scenario (see Sect. V):

- **Chirp start index** i_{start}
  Start index of the chirp. Valid range is from 0 to 511.
- **Chirp stop index** i_{stop}
  Stop index of the chirp. Valid range is from i_{start} to 511.
- **Number of loops** N_{loops}
  Number of times to repeat chirps from i_{start} to i_{stop} in each frame. Given that $N_{TX} = 2$ in the IWR1642, typically $i_{stop} - i_{start} = N_{TX}$. Hence, the total frame time T_{frame} follows as $T_{frame} = N_{TX} \cdot N_{loops} \cdot T_{c,c}$. The number of loops N_{loops} also defines the number of Doppler-FFT bins as $D = 2^{\lceil log_2 N_{loops} \rceil}$.
- **Number of frames** N_{frames}
  Number of frames to be transmitted. If $N_{frames} = 0$, the frames are transmitted infinitely long.
- **Frame periodicity** $T_{f,per}$
  Total time from start of one frame to the start of the next frame in ms. Hence, $T_{f,per}$ also defines the frame rate.

The chirp start index i_{start}, chirp stop index i_{stop}, and number of loops N_{loops} define the number of transmitted chirps. After the transmission of the frame the range/velocity/angle estimation as well as object detection can be performed. The whole procedure is repeated with the frame periodicity $T_{f,per}$.

C. Influence on radar performance

The parameters discussed in Sect. IV-A and Sect. IV-B highly influence the performance of the mmWave radar sensor for different environmental conditions. This section discusses these influences and derives equations to guide an optimal parameter selection. The maximum selectable bandwidth B for the Texas Instruments IWR1642 is 4 GHz when selecting the band from 77-81 GHz. Alternatively, one could also use the 76-77 GHz band with a bandwidth of 1 GHz (see Sect. III). As the ADC waits for the ADC valid start time $T_{ADC,valid}$ to acquire samples and stops after the ADC sampling time $T_{ADC,s}$, not the full bandwidth can be exploited, but the effective or ADC bandwidth B_{ADC} is defined as

$$B_{ADC} = S \cdot T_{ADC,s} \tag{17}$$

and hence can differ significantly from the theoretical bandwidth B. According to Eq. (7), the range resolution δd is

$$\delta d \approx \frac{c}{2 \cdot B_{ADC}} \text{ and} \tag{18}$$

the maximum detectable range d_{max} follows as

$$d_{max} \approx \frac{c \cdot f_{ADC,s}}{2 \cdot S}. \tag{19}$$

To derive the maximum relative velocity $v'_{r,max}$ of a FMCW radar system according to Eq. (10) it is necessary to calculate the wavelength λ'_S at the time when valid samples are available at the A/D converter, which is defined as

$$\lambda'_S = \frac{c}{f_S + S \cdot T_{ADC,valid}} \tag{20}$$

and the maximum relative velocity $v'_{r,max}$ follows as

$$v'_{r,max} = \frac{\lambda'_S}{4 \cdot T_{c,r}}. \tag{21}$$

Please note that $v'_{r,max}$ is not equal to $v_{r,max}$, as in Eq. (10) just a single TX antenna was considered. Finally, the velocity resolution δv depends on the total duration of the frame T_{frame} and follows as [14]

$$\delta v = \frac{\lambda'_S}{2 \cdot T_{frame}}. \tag{22}$$

Due to physical constraints it is impossible to maximize all the discussed performance metrics and hence one has to find a tradeoff depending on the use case as discussed in Sect. V.

Texas Instruments also provides a tool where these theoretical observations are visualized to select the desired chirp configuration. The tool is available online[5].

[5]https://dev.ti.com/gallery/view/1792614/mmWaveSensingEstimator/ver/1.3.0/

V. Scenario selection

Depending on the desired application and use case, a developer has to prioritize certain metrics discussed in Sect. IV-C to achieve the best performance and to fulfill the application requirements. For example, in a static setup, the velocity resolution δv might be less critical than the range resolution δd and the maximum detectable range d_{max}. Exemplarily, three different requirements/scenarios are discussed, namely (i) best range resolution (Sect. V-A), (ii) best velocity resolution (Sect. V-B), and (iii) best range (Sect. V-C). For each of these scenarios, the required radar system parameters as well as the tradeoffs are discussed. Please note that these scenarios are also selectable in the TI mmWave Demo Visualizer[6].

A. Best range resolution

In this generic scenario, the range resolution δd is the most critical requirement. Hence, the selected radar parameters have to ensure the best performance in a static or slowly changing environment, where highly precise and accurate range estimates to the objects are required. Typical applications include indoor mapping, power-line detection [7], or gesture recognition [5]. These applications have in common that the distance to the targets is relatively short.

The frame periodicity $T_{f,per}$ directly influences the frame rate, which should be kept high enough to capture slow movements in the scenario. However, a small frame rate reduces the CPU processing time and hence the energy consumption of the mmWave sensor. As discussed, the most critical requirement is the range resolution δd, hence, it is assumed that the separation between the objects is a minimum. According to Eq. (18), reducing the range resolution δd requires to increase the ADC bandwidth B_{ADC} and hence to increase the frequency slope S or the ramp end time $T_{ramp,end}$. Please note that, as discussed in Sect. IV-C, increasing the frequency slope S reduces the maximum detectable range d_{max}, the maximum relative velocity $v_{r,max}^{'}$ as well as the velocity resolution δv. Hence, the best range resolution might not be reachable if it is desired to also detect objects at higher distance or in situations where the radial velocities of the targets are increasing.

B. Best velocity resolution

The aim of this setup is to optimize the velocity resolution δv. Hence, it should support highly dynamic objects and environments as well as a high separation between targets with a similar radial velocity. Typical applications are radars for unmanned aerial vehicles and robots [4].

A low frame periodicity $T_{f,per}$ and high frame rate is required to enable high velocities. Thus, $T_{f,per}$ should be set as low as possible to still manage the high amount of processing data. This either requires high CPU power or highly efficient DSP algorithms. According to Eq. (22), maximizing the velocity resolution δv requires to minimize the ADC start wavelength $\lambda_S^{'}$ or to maximize the total frame time T_{frame}. The latter is achieved by increasing the number of loops N_{loops} in each frame and by increasing the chirp cycle time $T_{c,c}$ as discussed in Section IV-A. A higher $T_{c,c}$ requires to decrease the idle time T_{idle} and the ramp end time $T_{ramp,end}$. Depending on the application requirements and the expected velocity of the targets, the system designer might also have to optimize the maximum relative velocity $v_{r,max}^{'}$. According to Eq. (21), this requires to maximize the ADC start wavelength $\lambda_S^{'}$ and to minimize the chirp repetition period $T_{c,r}$. Thus, it is required to find a tradeoff since increasing the maximum relative velocity $v_{r,max}^{'}$ decreases the velocity resolution δv.

[6]https://dev.ti.com/gallery/view/mmwavebeta/mmWave_Demo_Visualizer_Record/ver/2.0.0/

C. Best range

This setup enables to unambiguously determine the distance to objects far away from the radar sensor. Hence, the aim is to maximize the detectable range d_{max} while maintaining a reasonable range resolution δd. Typical applications requiring this configuration are in outdoor environments, e.g., autonomous cars and driving assistance systems [6].

Similar to the *best range resolution* scenario, the frame rate should be chosen as low as possible to minimize data rate and processing overhead but high enough to support moving targets. The maximum detectable range d_{max} has to be high enough to detect targets at the farthest possible distance. In automotive applications this might be a distance of 50-100 m or maybe even further. According to Eq. (19), to increase d_{max}, a higher ADC sampling frequency $f_{ADC,s}$ or a smaller frequency slope S is required. Please note that decreasing the slope S reduces the range resolution δd, as discussed in Sect. V-A. Hence, detecting targets at higher distance lowers the capabilities of the radar sensor to separate between detected objects, requiring a tradeoff between maximum detectable range d_{max} and range resolution δd.

VI. Measurement Data

As mentioned in Sect. III, the IWR1642 chip employs a DSP subsystem to run the processing algorithms shown in the data processing chain in Fig. 8. Hence, the IWR1642 chip provides various measurement data, which can be further used for post-processing algorithms to build highly sophisticated radar applications. This section discusses the measurement data and performs evaluations in an indoor environment to showcase the information and its usability.

Range/Doppler heatmap. The range/Doppler heatmap consists of the detection matrix $\mathbf{A}$. The latter contains the results of the range-FFT d_i with $i = 0, \ldots, R-1$ and the results of the Doppler-FFT v_l with $l = 0, \ldots, D-1$. R is the number of range-FFT bins and D is the number of Doppler-FFT bins.

$$\mathbf{A} = \begin{bmatrix} (d_0, v_0) & \ldots & (d_0, v_{D-1}) \\ \vdots & & \vdots \\ (d_{R-1}, v_0) & \ldots & (d_{R-1}, v_{D-1}) \end{bmatrix} \tag{23}$$

Plotting the detection matrix $\mathbf{A}$ allows to visualize the velocity of a target over its distance to the radar.

List of detected objects. The IWR1642 provides a variable-length data structure containing information about each detected object. The latter consists of the index of the

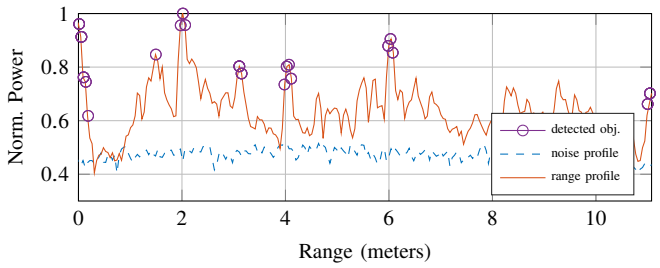

(a)

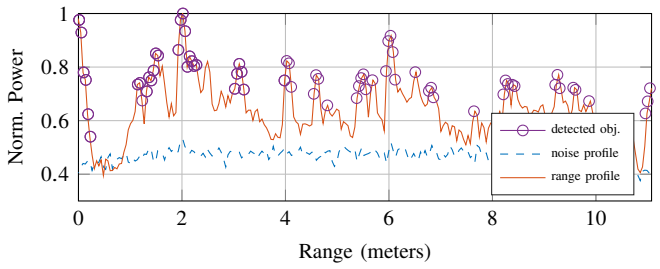

(b)

Fig. 10: Range profile (orange, solid), noise profile (blue, dashed), and detected objects (purple circles) in an indoor environment. At a distance of 2 m, a strong reflector was present. The threshold scale was set to 15dB (a) and 5dB (b).

range/Doppler bin in the detection matrix **A**, x/y/z coordinates, and a peak value [27]. The employed firmware (see Sect. III) uses a cell averaging constant false alarm rate (CA-CFAR) algorithm to detect the objects in the field of view of the radar [28], [29]. The task of the CFAR algorithm is to determine the power threshold above which a received signal can be assumed to originate from a certain object. If the threshold is set too low, more objects will be detected at the cost of a higher probability of false alarms. On the other hand, if the threshold is set too high, less objects will be detected and the number of false alarms will be lower. The CFAR algorithm aims to adapt the threshold level to maintain a constant probability of false alarms independently of a changing noise level due to clutter and interference. CA-CFAR marks a specific implementation of CFAR where the threshold is selected relative to a noise level in a reference window surrounding the sample/cell under test (CUT). The noise level is estimated by averaging the samples/cells in the reference window. The threshold is then selected as a function of the estimated noise level and a predetermined detection scale factor [29][7]. A measurement point will be considered as an object if the value of the CUT exceeds the threshold. The IWR1642 runs first a CFAR detection along the Doppler dimension and afterwards a range CFAR on the detected Doppler indices. Hence, it is possible to set different threshold scales in both dimensions [27].

Range profile. The range profile consists of the values of the detection matrix **A** at the 0th Doppler index, hence, it contains information about stationary objects. Its length is defined by the number of range-FFT bins R. Fig. 10 shows exemplarily two range profiles (orange, solid) acquired in a hallway at the University campus. The x-axis marks the range in meter and the y-axis the normalized power of the received signal. The IWR1642BOOST evaluation board was mounted on a desk at a distance of two meters from a strong reflector (over-head projector wall). The reflection from this reflector is prominent in the range profile at $d = 2\,m$. One can also see that other strong reflectors were present, which is to be expected in an indoor environment. Please note the strong peak at a very short distance to the radar (<0.2 m), which is due to antenna coupling. To compensate for this effect, the mmWave SDK provides the `calibDcRangeSig` function [26].

The purple circles in Fig. 10 mark the detected objects by the CA-CFAR algorithm. A threshold scale of 15 and 5 dB was used in Fig. 10a and Fig. 10b, respectively. It is evident that a lower threshold scale results in more detected objects. Furthermore, both figures clearly show the impact of the CA-CFAR algorithm, as the threshold is adapted for each sample depending on the power level in the reference window.

Noise floor profile. The noise floor profile contains the values of the detection matrix at the maximum Doppler index D and hence information about objects moving at the maximum speed. In the case of a stationary scene, there would be no objects present at this index: thus, the values represent the noise floor of the receiver. The length of the noise floor profile is equal to the number of range-FFT bins R. Fig. 10 (blue, dashed) shows the noise profile in a static setup.

Azimuth heatmap. The azimuth heatmap consists of the complex data for all virtual antennas[8] at the respective range bin. The values are derived from the *azimuth-FFT*, which is required for the angle of arrival estimation (see Sect. II-C), and from the range profile at the 0th Doppler index. Thus, strictly speaking, the acquired data composes the azimuth static heatmap. The structure of the azimuth static heatmap is defined by the following structure

$$\begin{bmatrix} (d_0, a_0) & \dots & (d_0, a_{N_v-1}) \\ \vdots & & \vdots \\ (d_{R-1}, a_0) & \dots & (d_{R-1}, a_{N_v-1}) \end{bmatrix} \tag{24}$$

where d_i $(i = 0, \dots, R-1)$ is the detection matrix **A** at the 0th Doppler index and a_l $(l = 0, \dots, N_v - 1)$ defines the index of the virtual antenna.

X-Y scatter plot. Besides the range/Doppler bin for the detection matrix **A**, the IWR1642 mmWave sensor provides x/y/z object coordinates incorporating also angular information. Please note that due to the antenna layout of the IWR1642BOOST evaluation board (see Fig. 7), just the azimuth angle is estimated, which limits the object detection to the 2D plane. On the other hand, the IWR1443 chip [30], i.e., the second 77 GHz radar sensor from TI's industrial mmWave family, has a third transmit antenna port. This enables to estimate also the elevation angle and to detect objects in the 3D-plane when using the IWR1443BOOST

[7]The TI IWR1642 chip allows to set the threshold scale via the `cfarCfg` command in the mmWave SDK [26].

[8]The number of virtual antennas N_v in a MIMO Radar is defined by the number of RX and TX antennas as $N_v = N_{TX} \cdot N_{RX}$ [16].

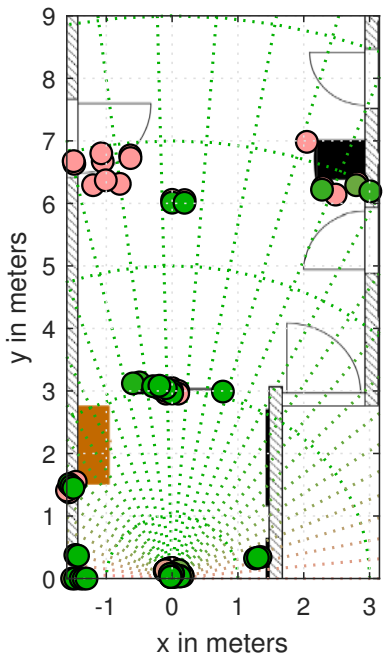

(a)

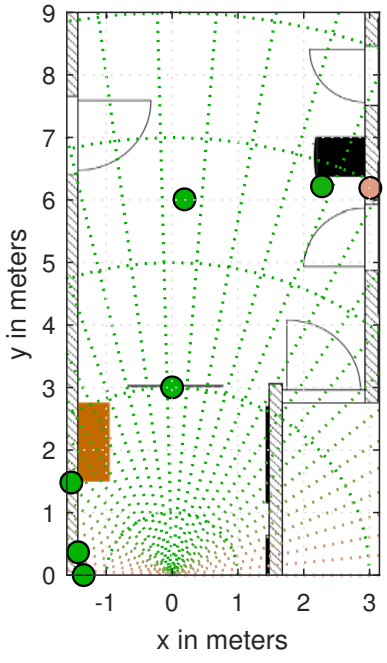

(b)

Fig. 11: X-Y scatter plot when the radar sensor is at a distance of 3 m from the reflecting wall. Green and red points mark targets that were detected in more and less than 10 % of the measurements, respectively. The experiments are performed with both peak grouping deactivated (a) and activated (b).

evaluation board [23]. The Cartesian coordinates can be used to present the detected objects in an intuitive manner to the user. Fig. 11a shows a X-Y scatter plot of a measurement in a hallway when the radar sensor was 3 meters apart from the strong reflector (over-head projector wall). The used profile was optimized for the *best range resolution* with a theoretical range resolution $\delta d = 4.36cm$ (see Sect. V-A). In total, 1000 measurements were performed. Green points mark targets that were detected in more than 10 % of all measurements. Red points mark targets that were detected in less than 10 % of the measurements and hence are assumed to be wrongly detected. The reflector at $d = 3m$ was clearly detected. Interestingly, also a target at a distance of $2 \cdot d = 6m$ was detected, which is due to double-reflections from the reflector. Also other perpendicular objects to the radar sensor where successfully detected, such as the shelves on the left side (brown rectangle) and a drink dispenser on the right side (black rectangle). As already shown in the range profiles in Fig. 10, close to the radar sensor (located at 0/0) multiple targets were detected falsely due to antenna coupling, which can be compensated using the the `calibDcRangeSig` function of the mmWave SDK.

Peak grouping. Besides the object detection and range/velocity/angle estimation, the TI IWR1642 supports a *peak grouping* feature. The latter groups detected neighboring peaks together to avoid multiple entries in the list of detected objects for the same physical target. Hence, instead of reporting a cluster of detected neighboring points, only one point, the one with the highest received signal strength, will be reported. This reduces the number of detected objects per measurement. Fig. 11b shows the results of 1000 measurements in the same experimental setup as in Fig. 11a, but this time the peak grouping feature was activated. Each of the clusters in Fig. 11a is now combined to a single detected target. For example, the strong reflector appears now as a single entry in the list of detected objects. Also the outliers at the door on the left side are removed.

Statistical information. This structure holds statistical information about the data path processing chain such as the CPU load (in %) during active/inter frame duration as well as timing information such as processing time and margins of the used profile. It enables to optimize the CPU usage and profile.

VII. Calibration

In the initial measurements, a range bias of a few centimeters has been observed, which is due to imperfections in the board and antenna layout. Hence, to enable highly accurate range measurements, it is required to run a calibration procedure beforehand to estimate the range bias of the individual mmWave platform. This range bias has to be subtracted from the range estimate at which the object was detected. The calibration procedure follows the following steps:

1) Mount the IWR1642BOOST evaluation kit in front of a strong reflector (e.g., metallic object) at a known distance d_{cal} (larger than 0.5 m) from the reflector.
2) The command `measureRangeBiasAndRxChanPhase` enables the measurement of the range bias as well as the receive channel gain and phase imperfections in the IWR1642 chip [26], [27]. The command requires as parameters: (i) the distance d_{cal} in meters between the reflector and the mmWave sensor (`targetDistance`) and (ii) the search window of the reflection originating from the strong reflector in the 0th Doppler index of the detection matrix (`searchWin`).

The search window is defined by the distance W in meters from `targetDistance`. The window size should be at least the size of a few range bins[9].

3) Start the radar measuring process using the `sensorStart` command.
4) The IWR1642 radar sensor provides the bias compensation data via the UART interface: the first value represents the range bias and the remaining values represent the phase bias as a complex value for each of the N_v virtual antennas.
5) The command printed at the UART interface (on the command line interface (CLI) port) has to be copied to the desired configuration file to compensate for the range as well as phase bias[10].

Within this report these compensation values were used:

```
compRangeBiasAndRxChanPhase 0.0751525 -0.74057
-0.62793 -0.62833 -0.64465 -0.69299 -0.68307
-0.71234 -0.70184 -0.45010 -0.64645 -0.33780
-0.63318 -0.39120 -0.69778 -0.40103 -0.71783
```

VIII. Conclusions and Future Work

The shift towards the millimeter-wave band enables numerous new applications for FMCW radars due to massive antenna arrays in a small area and the very large bandwidth. These properties combined with the availability of low-cost single-chip sensors from renowned semiconductor companies will make mmWave research affordable for many research groups.

This report is a comprehensive overview of FMCW mmWave radar sensors and their capabilities. It covers the basic principle of FMCW radars and discusses the low-level parameters of off-the-shelf sensors such as TI's IWR1642 chip. These parameters can be used as tuning knobs to maximize the system performance depending on environmental conditions and application requirements. Furthermore, the measurement data available after the processing chain of the IWR1642 radar sensor is discussed and initial evaluations are performed to showcase the potential of low-cost mmWave sensors for portable and mobile radar applications.

Future work will utilize the findings of this report to build a reliable radar-based indoor mapping system. For this purpose, it is meant to fuse the IWR1642 radar with sensors available in off-the-shelf smartphones and tablet PCs (e.g., accelerometer, magnetometer, and barometer). Besides the room geometry this also enables to derive reflective properties of the objects to support multipath-assisted localization systems.

IX. Acknowledgment

This work was supported by the Austrian Marshall Plan Foundation and the TU Graz LEAD project "Dependable Internet of Things in Adverse Environments".

[9]The mmWave SDK provides a configuration profile `profile_calibration.cfg` in `...\demo\xwr16xx\mmw\profiles` that can be used for the calibration process. Just d_{cal} and W have to be adjusted accordingly. One range bin in the configuration profile is about 5 cm, hence, $W = 0.2$ is a reasonable choice.

[10]When performing measurements without compensation, the following CLI command should be used: `compRangeBiasAndRxChanPhase 0.0 1 0 1 0 1 0 1 0 1 0 1 0 1 0 1 0`. This command sets the range bias to 0 and the phase coefficients to unity [27].

References

[1] C. Hülsmeyer, "Verfahren, um entfernte metallische Gegenstände mittels elektrischer Wellen einem Beobachter zu melden," *Eurpean Patent Office, Patentschrift DE165546*, vol. 30, 1904.

[2] R. Zhang and S. Cao, "Real-Time Human Motion Behavior Detection via CNN Using mmWave Radar," *IEEE Sensors Letters*, vol. 3, no. 2, Feb 2019.

[3] A. Ahmad, J. C. Roh, D. Wang, and A. Dubey, "Vital signs monitoring of multiple people using a FMCW millimeter-wave sensor," in *2018 IEEE Radar Conference (RadarConf18)*, April 2018, pp. 1450–1455.

[4] M. Caris *et al.*, "Synthetic aperture radar at millimeter wavelength for UAV surveillance applications," in *2015 IEEE 1st International Forum on Research and Technologies for Society and Industry Leveraging a better tomorrow (RTSI)*, Sep. 2015, pp. 349–352.

[5] P. Molchanov, S. Gupta, K. Kim, and K. Pulli, "Short-range FMCW monopulse radar for hand-gesture sensing," in *2015 IEEE Radar Conference (RadarCon)*, May 2015, pp. 1491–1496.

[6] J. Hasch *et al.*, "Millimeter-Wave Technology for Automotive Radar Sensors in the 77 GHz Frequency Band," *IEEE Trans. on Microwave Theory and Techniques*, vol. 60, no. 3, pp. 845–860, March 2012.

[7] Walabot, "Website," https://walabot.com/.

[8] Yu-Cheol Lee *et al.*, "Artificial landmark map building method based on grid SLAM in large scale indoor environment," in *2010 IEEE Intern. Conf. on Systems, Man and Cybernetics*, Oct 2010, pp. 4251–4256.

[9] B. Großwindhager *et al.*, "SALMA: UWB-based Single-Anchor Localization System Using Multipath Assistance," in *Proc. of the 16th ACM Conf. on Embedded Networked Sensor Systems*, ser. SenSys '18, 2018.

[10] A. Guerra *et al.*, "Application of transmitarray antennas for indoor mapping at millimeter-waves," in *2015 European Conference on Networks and Communications (EuCNC)*, June 2015, pp. 77–81.

[11] S. Hantscher *et al.*, "Localisation of concealed worn items using a millimeter wave FMCW radar," in *Asia-Pacific Microwave Conference 2011*, Dec 2011, pp. 955–958.

[12] C. Fiandrino, H. Assasa, P. Casari, and J. Widmer, "Scaling Millimeter-Wave Networks to Dense Deployments and Dynamic Environments," *Proceedings of the IEEE*, vol. 107, no. 4, pp. 732–745, April 2019.

[13] G. M. Brooker, "Understanding millimetre wave FMCW radars Understanding Millimetre Wave FMCW Radars," in *1st IEEE International Conference on Sensing Technology*. IEEE, 2005, pp. 152—-157.

[14] Texas Instruments, *White Paper. The fundamentals of millimeter wave sensors.*, 2017.

[15] M. I. Skolnik, *CW and frequency-modulated radar*. McGraw-Hill Book Company, Inc., 1962.

[16] Texas Instruments, *Application Report. MIMO Radar*, Texas Instruments, 2017.

[17] ——, "mmWave sensors," http://www.ti.com/sensors/mmwave/overview.html.

[18] Infineon, "RASIC Front-End IC's for Automotive RADARs," https://www.infineon.com/cms/de/product/sensor/radar-sensor-ics/.

[19] Texas Instruments, "Automotive mmWave sensors," http://www.ti.com/sensors/mmwave/awr/overview.html.

[20] ——, "Industrial mmWave sensors," http://www.ti.com/sensors/mmwave/iwr/overview.html.

[21] ——, *Datasheet. IWR1642 Single-Chip 76- to 81-GHz mmWave Sensor*, Texas Instruments, 2018.

[22] ——, *User's Guide. IWR1642 Eval. Module (IWR1642BOOST) Single-Chip mmWave Sensing Solution (Rev. A)*, Texas Instruments, 2018.

[23] T. Instruments, *User's Guide. IWR143BOOST Evaluation Module mmWave Sensing Solution (Rev. C)*, Texas Instruments, 2018.

[24] Texas Instruments, *User's Guide. DCA1000EVM Data Capture Card*, Texas Instruments, 2018.

[25] B. Großwindhager *et al.*, "Enabling Runtime Adaptation of Physical Layer Settings for Dependable UWB Communications," in *2018 IEEE 19th International Symposium on "A World of Wireless, Mobile and Multimedia Networks" (WoWMoM)*, June 2018, pp. 01–11.

[26] Texas Instruments, *User Guide. MMWAVE SDK. Product Release 2.0.0*, Texas Instruments, 2018.

[27] ——, *Millimeter Wave (mmw) Demo for XWR16XX. Doxygen Documentation*, Texas Instruments, 2018.

[28] H. Finn, "Adaptive detection mode with threshold control as a function of spatially sampled clutter level estimates," *RCA Rev.*, vol. 29, 1968.

[29] A. Jalil, H. Yousaf, and M. I. Baig, "Analysis of CFAR techniques," in *2016 13th International Bhurban Conference on Applied Sciences and Technology (IBCAST)*, Jan 2016, pp. 654–659.

[30] Texas Instruments, *Datasheet. IWR1443 Single-Chip 76- to 81-GHz mmWave Sensor*, Texas Instruments, 2017.